(3)

# THE INFLUENCE OF SHELL BEHAVIOR ON THE DESIGN OF LARGE ANTENNAS

by

J. W. MAR* and F. Y. M. WAN**

Massachusetts Institute of Technology, Cambridge, Massachusetts (U.S.A.)
Massachusetts Institute of Technology, Lexington, Massachusetts (U.S.A.)

## 1. Introduction

The most important structural requirement placed on large and highly accurate antennas is a very stringent restriction on the permissible change in the shape of the reflecting surface. "Large" in this context means diameters greater than fifty feet and "stringent" means that changes in shape are to be kept below approximately 1/16 of the operating wavelength. This leads to a deflection criterion on the order of 0.075 in. for operating frequencies of 10,000 Mc. A design requirement of this severity on the shape of such a large structure is highly unusual and not much information exists to assure its attainment.[1]

The main structural components of an antenna consist of a parabolic reflecting surface and a space-framework on which the reflector is mounted. If properly constructed, the reflector is a thin paraboloidal shell of revolution It is assumed that the antenna will be protected from wind loads by a radome so that the primary source of applied load is the dead weight of the structural components themselves. Long standing methods of analysis have been applied to study the structural capability of the space-frame,[7] but only very simple treatments of the reflecting surface have been conducted. Even with closed form solutions obtained by various approximate analyses, the accurate calculation of the deflections of the reflector is not easy since many complicated analytical expressions are involved.[2,3,4] Consequently, the intrinsic capabilities and advantages of shell actions have yet to be fully exploited. To this end a series of computer programs called LLAPS

* Professor of Aeronautics and Astronautics.

** Staff Member, Lincoln Laboratory (operated with support from the USAF).

The authors gratefully acknowledge the invaluable help given by Mrs. James SHEA of the Lincoln Laboratory in the preparation of this paper.

(Lincoln Laboratory Analyses of Paraboloidal Shells) has been developed by Lincoln Laboratory of Massachusetts Institute of Technology to calculate deflections as well as stresses of paraboloidal shells of revolution under the influence of gravity loads. Shells of a homogeneous material or of layer media including sandwich type construction can be handled. By means of these programs, the digital computer is utilized to evaluate the closed form solutions of the membrane, shallow shell and asymptotic approximations of general theory of thin elastic shells. Descriptions of these methods of solution and the solutions themselves have been published as Lincoln Laboratory reports and in part in Ref. 5. The present work discusses the implications of some of the results obtained by these programs. Our effort can be divided into three principal aspects. By introducing the concept of a moved focus, we establish in the first part of the paper a measure of the structural performance of the reflector and show that the structural capability of the shell, when viewed in proper context, is far better than that which appears at first sight. Next the effect of several design parameters on the structural behavior of the reflector is studied. Lastly, we discuss the existing method of construction of the parabolic reflector and offer an alternate concept suggested by the shell behavior. We confine ourselves to homogeneous and isotropic shells. The behavior of sandwich shells will be discussed in a future publication.

## 2. Root Mean Square Phase Error as a Measure of Antenna Performance

### The moved focus

The surface error of concern for the propagation of electromagnetic radiation is the additional path length which a ray must travel due to the distortion of the reflector. This additional path length is generally referred to as the **path length error** or the **phase error**. As we shall see, this phase error is intimately connected with the normal deflection of the middle surface of the undeformed shell and it will be shown that a part of this deflection is of the nature of rigid body motion. Evidently the rigid body components do not constitute a distortion of the paraboloidal reflecting surface in that they give rise to neither stretching nor bending strains. The deflection of the shell with the rigid body motion removed will henceforth be referred to as **pure distortion** or **effective deflection**. We may think of the deformation of the shell to be the sum of two separate processes: that of rigid body motion and that of pure distortion. We refer to the shell which has undergone only rigid body motions as the **moved paraboloid** and the shell which has undergone only pure distortion as the **distorted paraboloid**. Although rigid body, extensional and pure inextensional defor-

mations are qualitatively well understood, their influence on antenna design cannot be fully appreciated until numerical results are obtained. Calculations show that while the deflections relative to the undeformed shell as given by a linear bending shell analysis may be large, the pure distortion is at least an order of magnitude smaller except for a narrow region near the support(s). On the other hand, except for the slightly different orientation in space and therefore a slightly different location for the focal point, the moved paraboloid is in every other way the same as the undeformed reflecting surface. In particular, it has the same focal length. This suggests strongly that we should measure the structural capability of the reflector with respect to the moved paraboloid.

To do this we first derive a relation between the phase error with respect to the moved paraboloid and the normal deflection of the undeformed middle surface. This relation shows that the phase error is in fact proportional to the pure distortion of the undeformed shell. We then compute the root-mean-square of the phase error over the area of the reflecting surface. This single measure of surface deviation is generally used by radio-astronomers as a guide to the electromagnetic performance of the reflector. We shall use it as the basis for evaluating the structural performance of the reflector. Calculations show that the rms of the phase error with respect to the moved paraboloid is in fact at least an order of magnitude smaller than that with respect to the undeformed reflecting surface.

Thus our contribution in this aspect of our investigation lies in the recognition of the increase in the antenna performance to be gained by a consideration of the surface deviation from the moved paraboloid, which is the same as the undeformed reflecting surface except for the slightly different orientation in space, over that performance based on a consideration of the deformation relative to the undeformed reflector. To realize this gain, we must think of the focus of the reflector as having undergone a rigid body motion equivalent to that experienced by the moved paraboloid. For a given shell, this rigid body motion can be calculated by LLAPS.

## Geometry of shell

The middle surface of the antenna is a paraboloid of revolution. A point $o$ on the middle surface is located by rectangular Cartesian coordinates $y_1, y_2, y_3$ or by circular cylindrical coordinates $r, \theta, z$ (Fig. 1)

$$y_1 = r\cos\theta \tag{1}$$

$$y_2 = r\sin\theta \tag{2}$$

$$y_3 = z = \frac{r^2}{4f} \tag{3}$$

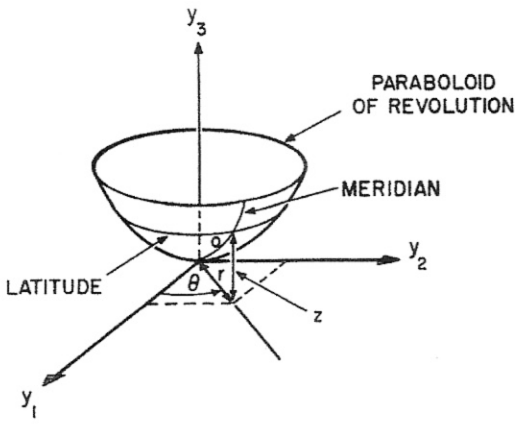


Fig. 1. Paraboloid of revolution

where $f$ is the focal length of the parabola (Fig. 2). Let

$$\gamma = \frac{r}{2f}. \tag{4}$$

Then the slope of the parabola (and therefore the slope of a meridian of the paraboloidal surface) is

$$\frac{dy_3}{dr} = \frac{r}{2f} = \gamma = \tan\phi \tag{5}$$

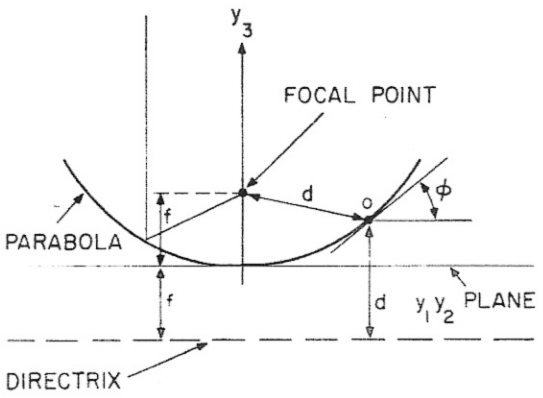


Fig. 2. Focal length of parabola

We shall use the dimensionless coordinates $\gamma$ and $\theta$ as our position coordinates. An element of arc length along a meridian (see Fig. 3) is

$$ds_r = 2f\sqrt{1+\gamma^2}\,d\gamma \tag{6}$$

while an element of arc length along a latitude (see Fig. 3) is

$$ds_\theta = 2f\gamma\,d\theta. \tag{7}$$

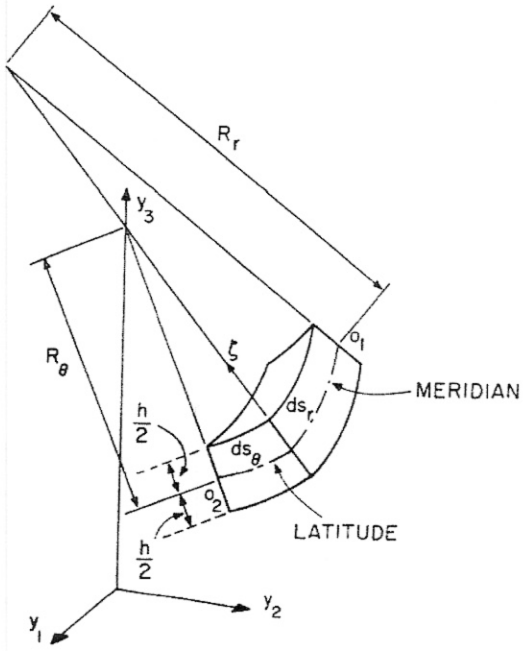


Fig. 3. Element of shell

An element of surface area on the middle surface is

$$dA = 4f^2\gamma\sqrt{1+\gamma^2}\,d\gamma\,d\theta. \tag{8}$$

With no loss in generality, we allow the antenna to rotate only about the $y_1$ axis and call the angle between $y_3$, the axis of revolution of the paraboloid, and the zenith the **pointing angle** $\psi$ (see Fig. 4). Steering the antenna in the azimuth direction has no bearing in our discussion.

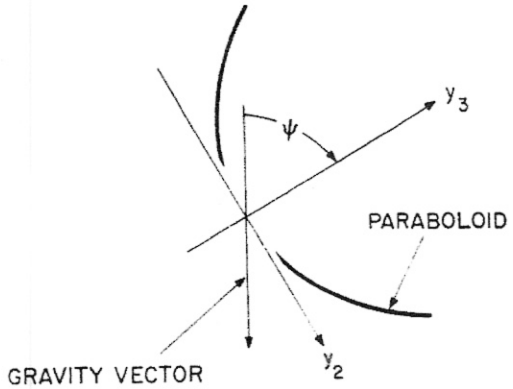


Fig. 4. Pointing angle

Other shell parameters of interest are as follows:

$u, v, w$ — components of mid-surface displacement (see Fig. (5));

$U, V, W$ — components of shell displacement (see Eqs. (9), (10) and (11));

$\omega_r, \omega_\theta$ — rotation of cross-section (see Fig. (5));

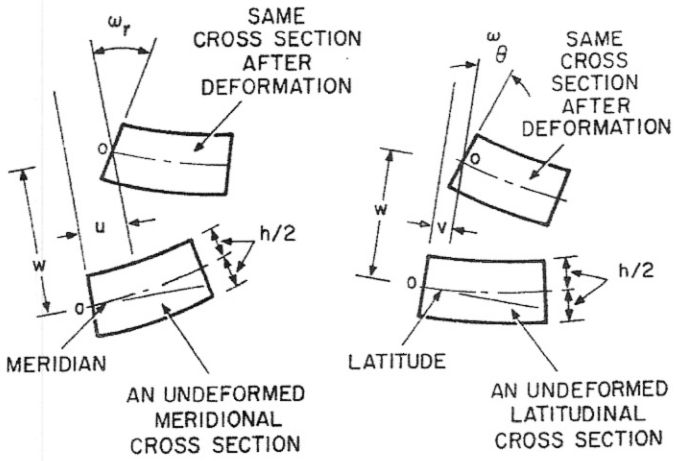


Fig. 5. Deformation of shell element

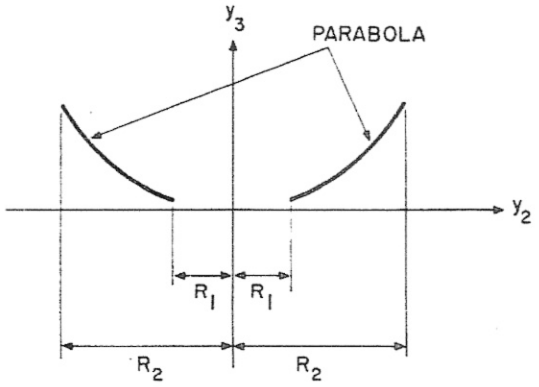


Fig. 6. Edges of shell

$h$ — thickness of shell (see Fig. (5));

$\zeta$ — shell coordinate in the direction of the midsurface normal $\vec{n}$ (see Fig. (3));

$R_r = 2f(1+\gamma^2)^{\frac{3}{2}}$ radius of curvature (see Fig. 3);

$R_\theta = 2f\sqrt{1+\gamma^2}$ radius of curvature (see Fig. 3);

$R_1, R_2$ — edges of shell (see Fig. 6);

$\rho_0$ — weight density of shell material;
$E$ — Young's Modulus;
$\nu$ — Poisson's ratio;
$\vec{i}_1, \vec{i}_2, \vec{i}_3$ — unit vectors associated with $y_1, y_2, y_3$;
$\phi = \tan^{-1}\gamma$ (see Fig. 2).

Under the usual Kirchhoff hypothesis, the deflection components $U$, $V$, and $W$ of the shell are given in terms of the deflection components of the middle surface $u$, $v$, and $w$ by

$$U = u - \zeta\omega_r \tag{9}$$

$$V = v - \zeta\omega_\theta \tag{10}$$

$$W = w \tag{11}$$

with $\omega_r$ and $\omega_\theta$ given in terms of combinations of $u, v, w$ and their derivatives.[4] Of particular interest is the relation between $W$ and $w$ which says that the normal deflection of the faces of the shell is the same as that of the middle surface. This fact simplifies our discussion considerably as $W$ is intimately related to the measure of the antenna performance. We shall speak of the normal deflection of the mid-surface, that of the shell, and that of the reflecting surface interchangeably.

**The normal deflection, $w$, due to gravity**

The displacement of the shell along a direction normal to the middle surface for the case of gravity loads can be expressed as[4]

$$w(\gamma, \theta) = w_s(\gamma)\cos\psi + w_a(\gamma)\sin\psi\sin\theta \tag{12}$$

where

$$w_s(\gamma) = \frac{4f^2\rho_0}{3E\sqrt{1+\gamma^2}}\left\{C_1^s f_1(\gamma) + C_2^s + f_3(\gamma) + \frac{(1+\gamma^2)^{\frac{7}{8}}}{\sqrt{\gamma}}\left[e^{\tau}(C_5^s\cos\tau + C_6^s\sin\tau) + e^{-\tau}(C_7^s\cos\tau + C_8^s\sin\tau)\right]\right\} \tag{13}$$

$$w_a(\gamma) = \frac{8f^2\rho_0}{E}\left\{C_1^a g_7(\gamma) + C_2^a g_8(\gamma) + C_3^a g_9(\gamma) + C_4^a g_{10}(\gamma) + g_{11}(\gamma) + \frac{(1+\gamma^2)^{\frac{3}{8}}}{\sqrt{\gamma}}\left[e^{\tau}(C_5^a\cos\tau + C_6^a\sin\tau) + e^{-\tau}(C_7^a\cos\tau + C_8^a\sin\tau)\right]\right\} \tag{14}$$

$$\tau = [3(1-\nu^2)]^{\frac{1}{4}}\sqrt{\frac{2f}{h}}\int^{\gamma}[1+\gamma^2]^{\frac{1}{4}}d\gamma \tag{15}$$

$$f_1(\gamma) = (1+\nu)\left[\sqrt{1+\gamma^2} - \ln\left(\frac{\sqrt{1+\gamma^2}}{\gamma}\right)\right] \tag{16}$$

$$f_3(\gamma)=\left\{(1+\nu)\left(\ln\gamma-\frac{1}{\gamma^2}\right)+\left(\frac{3-\nu}{2}\right)\gamma^2+\frac{\gamma^4}{4}+(1+\gamma^2)\left[\frac{1+\nu}{\gamma^2}-2(1-\nu)+\nu\gamma^2\right]\right\} \tag{17}$$

$$g_1(\gamma)=\frac{(1+\gamma^2)^{\frac{3}{2}}}{6}-(1+\nu)\left[\sqrt{1+\gamma^2}+\ln\left(\sqrt{1+\gamma^2}-1\right)-\ln(\gamma)\right] \tag{18}$$

$$g_2(\gamma)=\frac{(1-\nu)\gamma^2}{4}\ln\left(\frac{\sqrt{1+\gamma^2}-1}{\gamma}\right)+\frac{1-\nu}{4}\left(1+\sqrt{1+\gamma^2}\right)-\frac{(1+\nu)(1+\gamma^2)^{\frac{3}{2}}}{2\gamma^2} \tag{19}$$

$$g_3(\gamma)=\frac{\gamma^6}{360}-\frac{40+29\nu}{240}\gamma^4-\frac{1+\nu}{30\gamma^2}-\frac{1-\nu}{120}\gamma^2+\ln\gamma\left[\frac{(1-\nu)}{60}\gamma^2-\frac{1+\nu}{3}\right] \tag{20}$$

$$g_4(\gamma)=\frac{g_1(\gamma)}{\sqrt{1+\gamma^2}}-\frac{\gamma f_1^*(\gamma)}{\sqrt{1+\gamma^2}}-(1+\nu) \tag{21}$$

$$g_5(\gamma)=\frac{g_2(\gamma)}{\sqrt{1+\gamma^2}}-\frac{\gamma f_2^*(\gamma)}{\sqrt{1+\gamma^2}}+\frac{2(1+\nu)}{\gamma^2} \tag{22}$$

$$g_6(\gamma)=\frac{g_3(\gamma)}{\sqrt{1+\gamma^2}}-\frac{\gamma f_3^*(\gamma)}{\sqrt{1+\gamma^2}}+\frac{2(1+\nu)(1-4\gamma^2)(1+\gamma^2)^{\frac{3}{2}}}{15\gamma^2} \tag{23}$$

$$g_7(\gamma)=\frac{1}{\gamma}\left\{g_4(\gamma)-\sqrt{1+\gamma^2}g_1(\gamma)-\frac{(1+\nu)}{2}-\frac{\nu\gamma^2}{2}\right\} \tag{24}$$

$$g_8(\gamma)=\frac{1}{\gamma}\left\{g_5(\gamma)-\sqrt{1+\gamma^2}g_2(\gamma)-\frac{(1+\nu)}{\gamma^2}-\nu\right\} \tag{25}$$

$$g_9(\gamma)=-\frac{\gamma}{\sqrt{1+\gamma^2}}\left(1+\frac{\gamma^2}{2}\right) \tag{26}$$

$$g_{10}(\gamma)=-\frac{\gamma}{\sqrt{1+\gamma^2}} \tag{27}$$

$$g_{11}(\gamma)=\frac{1}{\gamma}\left\{g_6(\gamma)-\sqrt{1+\gamma^2}g_5(\gamma)-\frac{\sqrt{1+\gamma^2}}{\gamma^2}\left[\frac{\gamma^4}{2}+\frac{(1+\gamma^2)^2}{15}+\frac{\nu(1+\gamma^2)^3}{15}\right]\right\} \tag{28}$$

$$f_1^*(\gamma)=\sqrt{1+\gamma^2}\left(\frac{\gamma}{2}-\frac{1+\nu}{\gamma}\right) \tag{29}$$

$$f_2^*(\gamma)=\frac{(1+\nu)\sqrt{1+\gamma^2}}{\gamma^3}\left(1-\frac{\gamma^2}{2}\right)+\frac{(1-\nu)\gamma}{2}\left[\ln\left(\sqrt{1+\gamma^2}-1\right)-\ln(\gamma)\right] \tag{30}$$

$$f_3^*(\gamma)=\frac{(1-\nu)}{3}\gamma\ln(\gamma)+\frac{(1+\nu)}{15\gamma^3}-\frac{(1+\nu)}{3\gamma}-\frac{(40+29\nu)}{60}\gamma^3-\frac{\gamma^5}{60}. \tag{31}$$

The function $w_s(\gamma)$ represents the deflection of the antenna in the direction normal to the middle surface when it is pointed at the zenith and $w_a(\gamma)$ is

the same deflection along the radius located by $\theta = \pi/2$ when the antenna is pointed at the horizon. These are sometimes referred to as the "face-up" and "face-side" positions, respectively.

The effect of the components of the solution associated with the constants $C_5$, $C_6$, $C_7$ and $C_8$ is confined to a narrow region near the edge(s) of the shell provided the structural parameter $k$ is large compared to unity and is therefore referred to as the **edge zone solution**. $k$ is given in terms of the shell geometry by

$$k^4 = \frac{R_s^4 C}{DR^2} = \frac{R_s^4}{4f^2h^2} 12(1-\nu^2) \tag{32}$$

where $C$ and $D$ are the stretching and bending stiffness of the shell respectively, $R_s$ is the value of $r$ at the support, and $R$ is the representative magnitude of the radii of curvature (and is equal to $2f$ for our paraboloid). The remaining solution components are "slowly varying" functions of $\gamma$. We shall refer to them as the **membrane solutions** to conform with the conventional engineering terminology although **interior solution** would be more appropriate. Within the membrane solution, those associated with $C_2^s$, $C_3^a$ and $C_4^a$ are the so-called **inextensional** components while the balance is referred to as the **extensional** components.

It can be ascertained from Ref. 4 that the rigid body components of the solution do not appear in the expressions for the stress resultants and bending moments. Thus, they represent deflections due to rigid body translations along the $y_2$ and $y_3$ axes, and rigid body rotation about the $y_1$ axis. To see this more directly, let the antenna be given a small rigid body motion

$$\vec{\Delta} = [\Delta_2 + z\mathcal{H}]\vec{i}_2 + [\Delta_3 - r\sin\theta\mathcal{H}]\vec{i}_3 \tag{33}$$

where $\Delta_2$ and $\Delta_3$ represent rigid body translations along the $y_2$ and $y_3$ axes respectively and $\mathcal{H}$, a rotation about the $y_1$ axis. In view of our definition for the pointing angle $\psi$, they are the only possible rigid body motions. These rigid body motions give rise to a normal displacement $w_{rb}$.

$$\begin{aligned} w_{rb} &= \Delta_3\cos\phi - (\Delta_2 + z\mathcal{H})\sin\theta\sin\phi + (\mathcal{H}r\sin\theta)\cos\phi \\ &= \Delta_3\left(\frac{1}{\sqrt{1+\gamma^2}}\right) - \Delta_2\left(\frac{\gamma\sin\theta}{\sqrt{1+\gamma^2}}\right) \\ &\quad + 2f\mathcal{H}\left(1+\frac{\gamma^2}{2}\right)\frac{\gamma\sin\theta}{\sqrt{1+\gamma^2}}. \end{aligned} \tag{34}$$

Thus, expressions in the normal deflection $w$ of the shell having the form $\frac{1}{\sqrt{1+\gamma^2}}$, $\frac{\gamma\sin\theta}{\sqrt{1+\gamma^2}}$, and $\frac{\gamma^3\sin\theta}{\sqrt{1+\gamma^2}}$ are of the nature of rigid body motions. In particular, terms associated with $C_2^s$, $C_3^a$ and $C_4^a$ (i.e., the inextensional components) are just such expressions as we have set out to show. Moreover,

it is not difficult to see that the extensional components of the shell solution also have a rigid body content. In the face-up position, the rigid body deflection is a translation parallel to the $y_3$ axis. In the face-side position, the rigid body deflection consists of a translation in the direction of the $y_2$ axis plus a rotation about the $y_1$ axis. At intermediate pointing angles, all three components will be present.

There are several ways to characterize the deformation of shells under the action of gravity loads. As a natural consequence of the above discussion, let us first consider the complete deformation as the sum of a membrane part and an edge zone part. These two effects may be viewed as occurring in sequence. Consider first a parabolic antenna in the face-up position and supported as shown in Fig. 7. The interior boundary $R_1$ is simply-supported

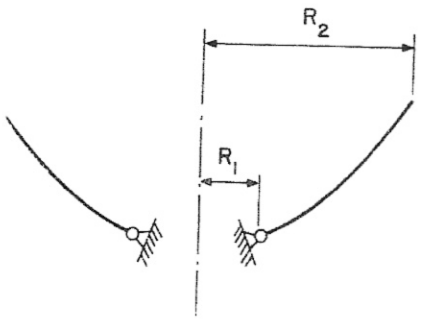


Fig. 7. Shell simply-supported at inner edge

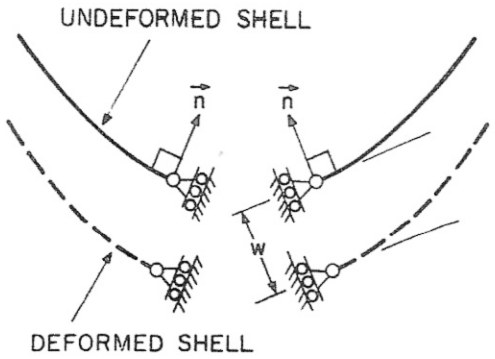


Fig. 8. Boundary conditions for membrane behavior

and the outer boundary $R_2$ is free. Under gravity loads the shell, in its membrane action alone, behaves as if it has rollers at $R_1$ as shown in Fig. 8. If the actual physical supports were of this type, then the deformed position of the shell is as shown schematically by the dotted lines in the same figure. The actual normal displacement calculated by a membrane analysis[2] is given

as a function of position by the curve labeled "membrane" in Fig. 9. Clearly much of the displacement shown can be arrived at by translating the antenna surface as a rigid body.

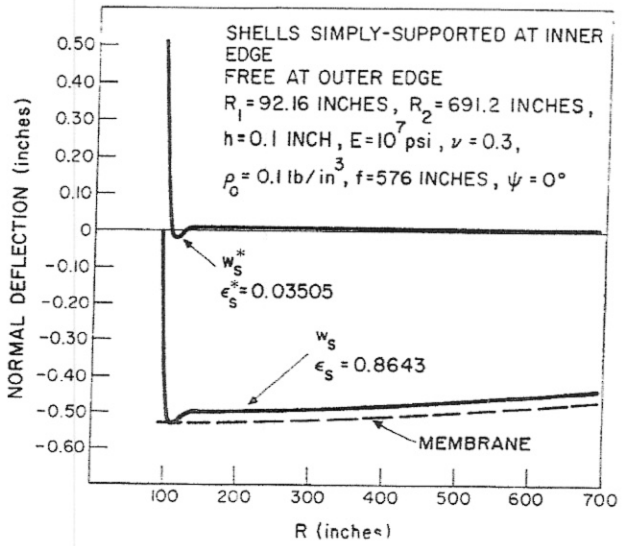


Fig. 9. Deflection curves

Roller supports of the type shown in Fig. 8 are difficult to achieve. The mathematical satisfaction of the zero displacement boundary conditions shown in Fig. 7 is achieved by adding an edge zone solution to the membrane

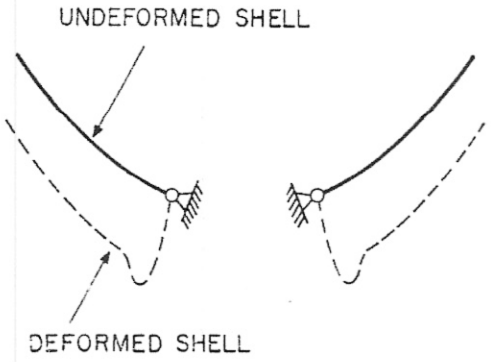


Fig. 10. Sketch of face-up shell behavior

solution. Figuratively, the effect of the edge zone solution is to push the roller supports back to their undeflected position. This in turn affects the mode of deformation of the rest of the shell, yielding the final deformed shape shown as the dashed line in Fig. 10. The complete solution for $w_s$

obtained in Ref. 4 is given as a function of position by the curve labeled $w_s$ in Fig. 9. It is seen that the dominant effect of pushing the roller supports back to their undeformed position is local in that it is confined to a narrow region near the edge $R_s = R_1$. Figure 10 shows schematically that a rigid body translation can achieve the deflection over a large part of the shell. The result of removing such a translational motion is labeled $w_s^*$ in Fig. 9. This is equivalent to moving the focal point of the undeformed paraboloid to a new position in space without changing the focal length. With respect to the new focal point, the deformed reflector is almost a perfect paraboloid with the region of maximum displacements now located near the supports. However, the area over which the $w_s^*$ displacements are large must be an edge zone phenomenon in view of the above discussion. In the face-side position the same sort of a phenomenon occurs. As shown schematically in Fig. 11 the unsymmetrical nature of the loads causes the membrane

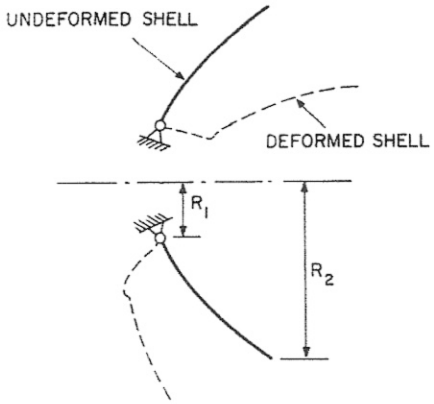


Fig. 11. Sketch of face-side shell behavior

behavior to cause inward deflections over the top half of the shell and outward deflections over the bottom half. It can be seen that the rigid body deflections are due to a combination of translation plus rotation. Numerical results equivalent to those given in Fig. 9 will be omitted for the face-side position because we shall see them later in Sec. 3.

In summary, we have now presented the (asymptotic) normal deflection of the shell by a linear bending shell analysis and shown that much of this deflection is of the nature of rigid body motions and that the balance is effectively an edge zone phenomenon. Instead of the previous edge zone and membrane consideration, we shall henceforth view the deformation of the shell as the sum of two separate processes: the rigid body motion $w_{rb}$ and the pure distortion $w^*$. We shall use these results to establish a measure of the antenna performance in the next two subsections.

**The phase error**

The surface error of concern for the propagation of electromagnetic radiation is the additional path length which a ray must travel due to distortions. In Fig. 12, points $r$ and $s$ are on the surface of the undeformed parabola, and $p$ is on the deformed parabola. A ray from the focal point

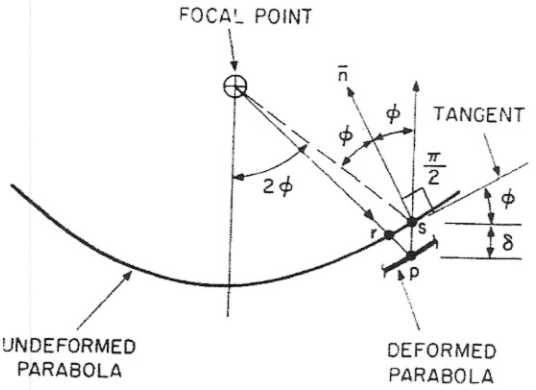


Fig. 12. The axial error

traverses through points $r$, $p$ and $s$. For small deviations, the distance $rp$ is negligibly different from $ps$ which is referred to as the axial error and will be denoted by $\delta$. This results in a **path length error**[6] or phase error given by

$$e = \delta(1+\cos 2\phi). \tag{35}$$

The total deformation of the antenna surface, as has been pointed out, includes a rigid body component. By associating a motion of the focal point with the rigid body component, the electromagnetic performance of the antenna can be measurably improved because the path length error will be less. This will now be shown. The derivations, which will entail a slight amount of geometry, are based on Fig. 13 with the terminology already established as well as the following additional nomenclature:

$f_0$ — initial location of focal point;
$F_0$ — location of focal point of the moved paraboloid;
$p$ — point on undeformed antenna surface;
$P$ — position of $p$ after deformation;
$q$ — position of $p$ due to rigid body motions;
$Q$ — axial projection of $P$ on the moved paraboloid;
$\vec{j}_2, \vec{j}_3$ — unit vectors associated with $\tilde{y}_2$, $\tilde{y}_3$ axes, resp.;
$\Delta r$ — increment in $r$ of the moved paraboloid due to pure distortion;
$\vec{u}$ — displacement vector of the middle surface of the undeformed shell;
$\vec{\Delta}$ — the rigid body portion of $\vec{u}$.

A point $p$ on the surface of the antenna under the action of the gravity loads deflects to point $P$. Using the initial location of the focal point $f_0$, the axial error is given by the $y_3$ component of the vector $\vec{u}(pP)$. The rigid body component $\vec{\Delta}$ of this displacement vector enables us to locate the

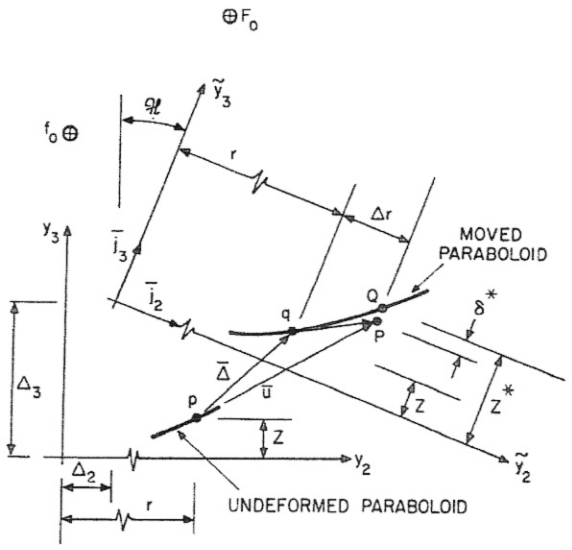


Fig. 13. Axial error of the moved paraboloid

position of the moved paraboloid as well as its focus $F_0$. Let $Q$ be the projection of $P$ on the moved paraboloid along the direction $y_3$ (the axis of revolution of the moved paraboloid). Then the distance $z^*$ from $Q$ to the $y_1y_2$ plane is given by

$$z^* = \frac{(r+\Delta r)^2}{4f} = \frac{r^2}{4f} + \Delta r \tan\phi. \tag{36}$$

$\Delta r$ is sufficiently small (since it is of the same order of magnitude as $u$, $v$ and $w$) such that $(\Delta r)^2$ can be neglected. Then, with respect to the moved paraboloid, the axial error is the distance $PQ$ which will be labeled $\delta^*$. An examination of Fig. 13 reveals

$$\delta^* = z^* - z - \vec{j}_3 \cdot (\vec{u} - \vec{\Delta}) \tag{37}$$

$$\Delta r = \vec{j}_2 \cdot (\vec{u} - \vec{\Delta}) \tag{38}$$

$$z^* - z = \Delta r \tan\phi. \tag{39}$$

The displacement vector is expressed as

$$\begin{aligned}\vec{u} = {} & [u\cos\phi\cos\theta - v\sin\theta - w\sin\phi\cos\theta]\vec{i}_1 \\ & + [u\cos\phi\sin\theta + v\cos\theta - w\sin\phi\sin\theta]\vec{i}_2 \\ & + [u\sin\phi + w\cos\phi]\vec{i}_3.\end{aligned} \tag{40}$$

Terms like $u\mathcal{H}$, $\mathcal{H}\Delta_2$, etc. can be neglected; there results

$$\delta^* = w(-\tan\phi\sin\phi-\cos\phi)-(z\mathcal{H}+\Delta_2)\sin\theta\tan\phi-\mathcal{H}r\sin\theta+\Delta_3. \quad (41)$$

By equation (33), we can write (39) as

$$\delta^* = -\frac{1}{\cos\phi}(W-W_{rb}) \quad (42)$$

where $w_{rb}$ is the normal component of the rigid body motion of the shell which is the same as the rigid body motion experienced by the moved paraboloid and its focus. Note that if $\vec{\Delta} = 0$, then

$$\delta^* = \delta = -\frac{w}{\cos\phi}. \quad (43)$$

Since $w$ has the form shown by Eq. (8) it is convenient to write

$$\delta^* = \delta_s^*(\gamma)\cos\psi+\delta_a^*(\gamma)\sin\psi\sin\theta. \quad (44)$$

This leads to

$$\delta_s^* = -\frac{w_s^*}{\cos\phi} \quad (45)$$

$$\delta_a^* = -\frac{w_a^*}{\cos\phi} \quad (46)$$

where

$$w_s^* = w_s-\Delta_3\cos\phi \quad (47)$$

$$w_a^* = w_a+\sin\phi(\Delta_z+z\mathcal{H})+\cos\phi(\mathcal{H}r\sin\theta). \quad (48)$$

The quantities $w_s^*$ and $w_a^*$ are measures of pure distortion in the direction normal to midsurface. It was shown that they are in fact an order of magnitude smaller than $w_s$ and $w_a$, respectively, except for a narrow edge zone. Therefore, we expect in general $\delta^*$ to be also an order of magnitude smaller than $\delta$ (see Eqs. 42 and 43) except for the same edge zone.

The path length error or phase error (see Eq. 34) can also be defined with respect to the moved paraboloid

$$e^* = \delta^*(1+\cos 2\phi). \quad (49)$$

**The root-mean-square of the phase error**

The path length error given by Eq. (49) varies from point to point. A useful single measure of surface deviation is the root-mean-square value defined by

$$\varepsilon^* = \left\{\frac{4f^2}{A}\int_0^{2\pi}\int_{\gamma_1}^{\gamma_2}(e^*)^2\gamma\sqrt{1+\gamma^2}\,d\gamma\,d\theta\right\}^{\frac{1}{2}} \quad (50)$$

where $A$ is the total surface area of the midsurface, i.e., the integral of (8). This can be put into the form

$$\varepsilon^* = \{(\varepsilon_s^*)^2\cos^2\psi+(\varepsilon_a^*)^2\sin^2\psi\}^{\frac{1}{2}} \quad (51)$$

where

$$\varepsilon_s^* = \left\{ \frac{32\pi f^2}{A} \int_{\gamma_1}^{\gamma_2} [w_s^*]^2 \frac{\gamma d\gamma}{\sqrt{1+\gamma^2}} \right\}^{\frac{1}{2}} \tag{52}$$

$$\varepsilon_a^* = \left\{ \frac{16\pi f^2}{A} \int_{\gamma_1}^{\gamma_2} [w_a^*]^2 \frac{\gamma d\gamma}{\sqrt{1+\gamma^2}} \right\}^{\frac{1}{2}}. \tag{53}$$

Similarly, if the rigid body motion is included, then the measure of surface deviation becomes

$$\varepsilon = \left\{ \frac{4f^2}{A} \int_0^{2\pi} \int_{\gamma_1}^{\gamma_2} (e)^2 \gamma \sqrt{1+\gamma^2} d\gamma d\theta \right\}^{\frac{1}{2}} \tag{54}$$

or

$$\varepsilon = \{(\varepsilon_s)^2 \cos^2 \psi + (\varepsilon_a)^2 \sin^2 \psi\}^{\frac{1}{2}} \tag{55}$$

where

$$\varepsilon_s = \left\{ \frac{32\pi f^2}{A} \int_{\gamma_1}^{\gamma_2} [w_s]^2 \frac{\gamma d\gamma}{\sqrt{1+\gamma^2}} \right\}^{\frac{1}{2}} \tag{56}$$

$$\varepsilon_a = \left\{ \frac{16\pi f^2}{A} \int_{\gamma_1}^{\gamma_2} [w_a]^2 \frac{\gamma d\gamma}{\sqrt{1+\gamma^2}} \right\}^{\frac{1}{2}}. \tag{57}$$

These root-mean-square values of the surface deviations will be used as the basis for evaluating the effect of shell behavior on the design of large antennas.

By simple consideration of the areas under the appropriate curves, it is not difficult to see (at least intuitively) that $\varepsilon^* \leqslant \varepsilon$. For the example given in Fig. 9, we have

$$\varepsilon = 0.8643 \tag{58}$$

$$\varepsilon^* = 0.03505 \tag{59}$$

Later results show that $\varepsilon^*$ is consistently an order of magnitude smaller than $\varepsilon$.

### 3. The Effect of Some Design Parameters

We shall show in this section the effect of some design parameters on the root-mean-square of the phase error which has been established as a performance criterion. The parameters to be examined are entitled (a) material, (b) size, (c) thickness, (d) focal length, (e) location of the inner boundary, (f) type of support, and (g) interior support. Additionally, a few curves of the actual and effective normal deflection will be shown.

**Material**

Assuming the material is homogeneous and isotropic, the deflection as well as the RMS phase error is a linear function of the material parameter $\rho_0/E$ just as is the case discussed in Ref. 5. This is to be expected because both $\rho_0$ and $E$ appear only as linear factors in the load terms. It is therefore not necessary to display any data since minimum values of displacement and phase error will be obtained with the material with the largest value of $E/\rho_0$.

**Size**

The ability of a shell structure to carry its own dead weight with very little distortion is evident in Figs. 14 and 15. Deflection curves for four shells, simply-supported at outer radii of 230.4, 460.8, 921.6 and 1382.4 in. respectively, and closed at the apex, are shown. Note that the maximum deflection is not a strong function of the size, i.e., of the outer radii. This

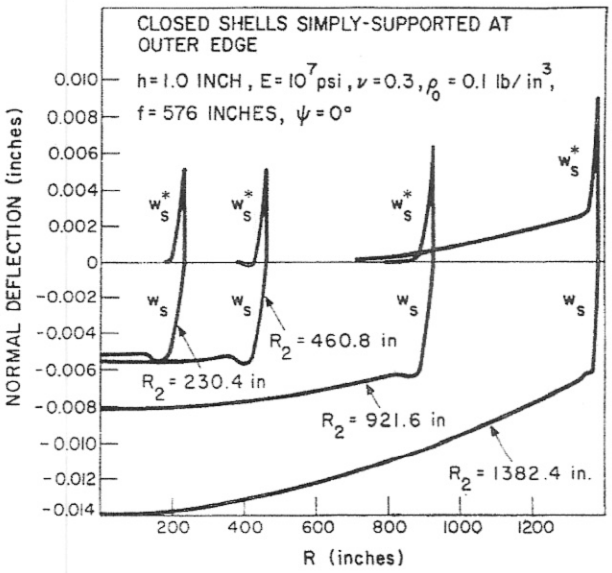


Fig. 14

is in contrast to the usual beam, plate or truss structures wherein maximum deflections are generally proportional to the fourth power of a characteristic length dimension. The shell carries its loads primarily as a membrane with a minimum of bending and this is the reason for the relatively small deflections.

Curves of $w^*$ are also shown in Figs. 14 and 15. The root-mean-square values of the phase error are shown for both the $w$ and $w^*$ curves in Fig. 16.

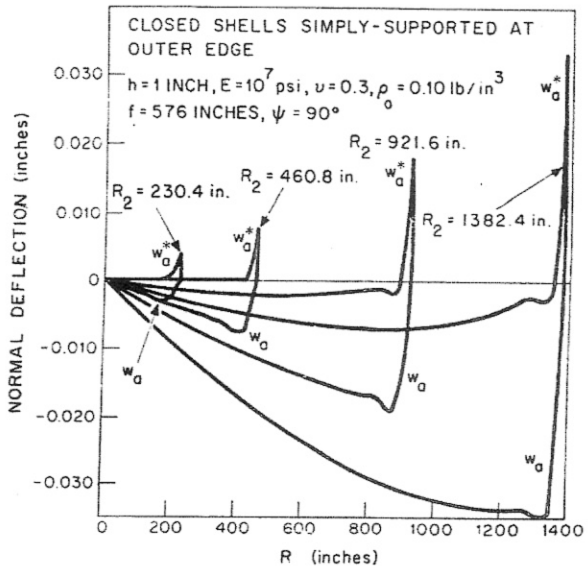


Fig. 15

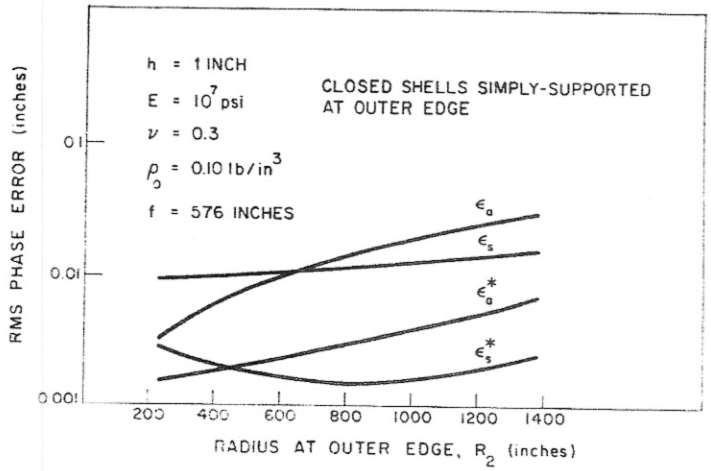


Fig. 16

(A logarithmic scale has been used since several orders of magnitude are encompassed by the RMS numbers.) The larger value of $\varepsilon^*$ for the 230.4 in. shell in the face-up attitude as compared to the 460.8 and 921.6 in. ones is due to the increased role of the edge bending for the smaller shell. The width of the edge zone is approximately the same for the four shells and, hence, the percent of the shell affected by bending is greatest for the smallest shell. Note that the deflections in the face-side attitude ($\psi = 90°$) are larger than in the face-up attitude ($\psi = 0°$) for all but the 230.4 in. shell.

Four other shells, simply-supported at the same inner radii of 100 in. and free at outer radii 300, 400, 600 and 800 in. respectively, have been analyzed and the results are shown for the face-up and face-side attitudes in Figs. 17 and 18, respectively. As in Fig. 14, the deflections shown in Fig. 17 for the face-up position are not a strong function of size. But, in

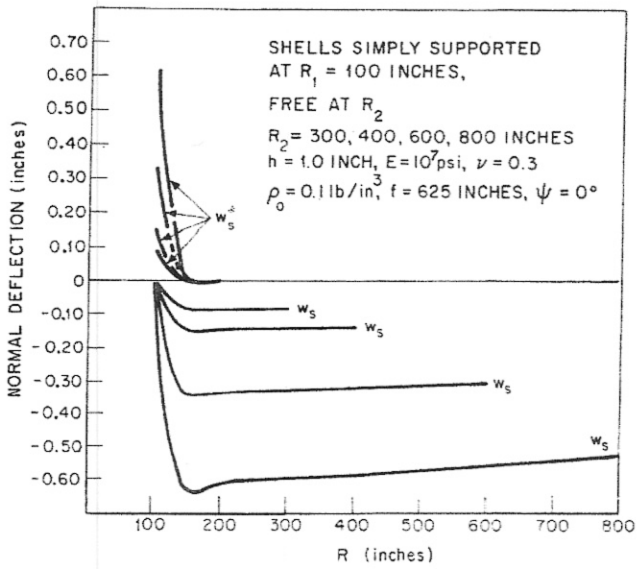


Fig. 17

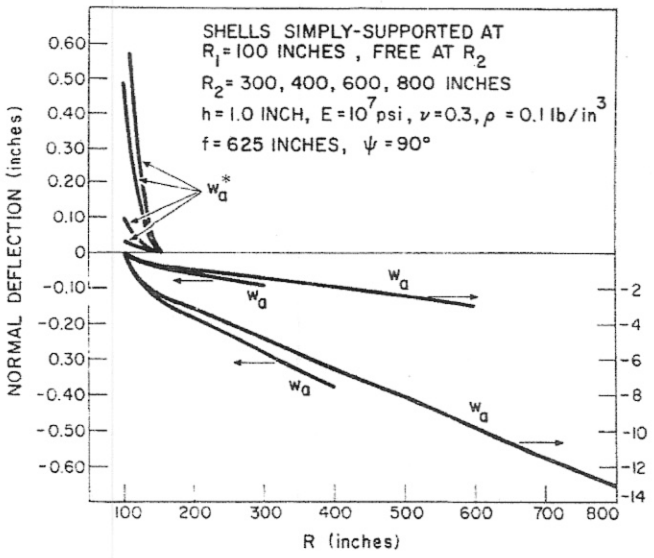


Fig. 18

the face-side attitude the maximum deflections shown in Fig. 18 are a very strong function of size. However, the effective displacement $w^*$ is a much weaker function of size than is the total deflection $w$. The RMS values are plotted against the outer radius in Fig. 19.

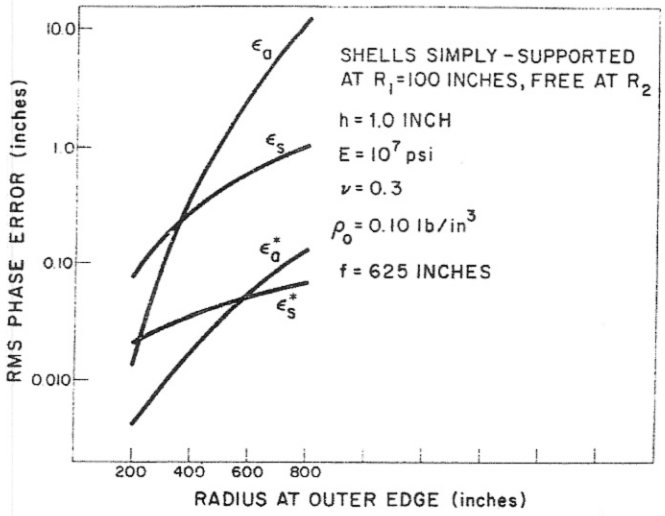


Fig. 19. Effect of outer radius

It is evident from these results that a shell is much stiffer if the support is at the outer edge (a shell closed at the apex and a shell with an inner hole free of support exhibit little difference in their mode of deformation). But this increase in stiffness must be balanced by the difficulties encountered in the construction of a support at a large radius and by the degree to which the ideal simple-support conditions can be attained.

**Thickness**

The thickness, $h$, determines the extensional and bending stiffness of the shell, and, since only gravity loads are being considered, also the loading. If the bending stiffness is neglected (i.e., assume membrane behavior) then the deflections turn out to be independent of thickness for gravity loads.[2] Five shells, differing only in their thickness, were analyzed. The shells were simply supported at a radius of 92.16 in. and free at a radius of 691.2 in. Curves of the root-mean-square values of the total deflection $w$ and the effective deflection $w^*$ are shown in Fig. 20 for the symmetric ($\psi = 0°$) and antisymmetric ($\psi = 90°$) cases. The RMS values of the phase error based on $w$ decrease slightly with increasing thickness whereas the RMS values based on $w^*$ increase with increasing thickness. The former is true because

the increase in bending stiffness with thickness decreases the deflections in the edge zone. The latter occurs because the width of the edge zone (wherein the largest $w^*$ occurs) becomes narrower as bending stiffness decreases. Thus, the smallest value of $\varepsilon^*$ is obtained for a shell of zero bending stiffness,

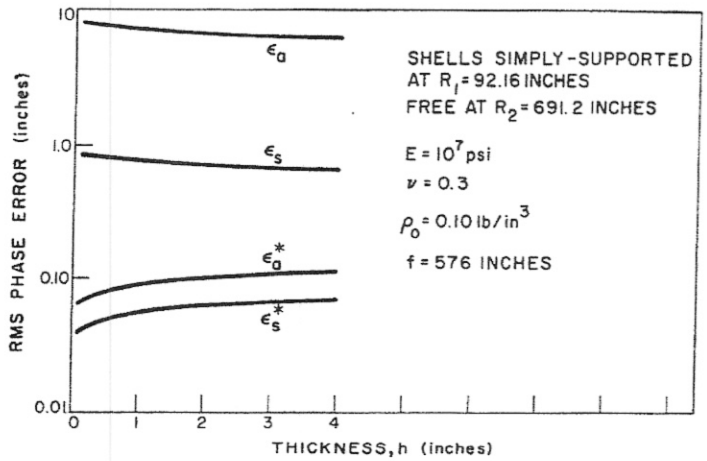


Fig. 20. Effect of thickness

i.e. of zero thickness. Even though the face-side deflections are an order of magnitude larger than those for the face-up position, the RMS values of the corresponding phase errors of the effective deflections are of the same order of magnitude.

### Focal length

The effect of the focal length can be examined from two different points of view. We can hold $R_1$ and $R_2$ fixed and vary $f$ so that $\gamma_1$ and $\gamma_2$ change with $f$. This was done in Ref. 5 and will not be repeated here. Alternately, we can hold $\gamma_1$ and $\gamma_2$ fixed so that $R_1$ and $R_2$ change with $f$. Therefore, implicit in this second alternative is also a change in size. We have studied a series of geometrically similar shells which are simply-supported at $\gamma_1 = 0.08$ and free at $\gamma_2 = 0.6$. Results are shown in Fig. 21. It is observed that all of the four curves vary approximately as the square of the focal length. Note again the two orders of magnitude difference between $\varepsilon$ and $\varepsilon^*$.

### Location of inner boundary

Two different groups of shells are considered in this section. These shells are similar in configuration to those studied earlier except that the outer boundary is fixed and the size is varied by changing the inner boundary.

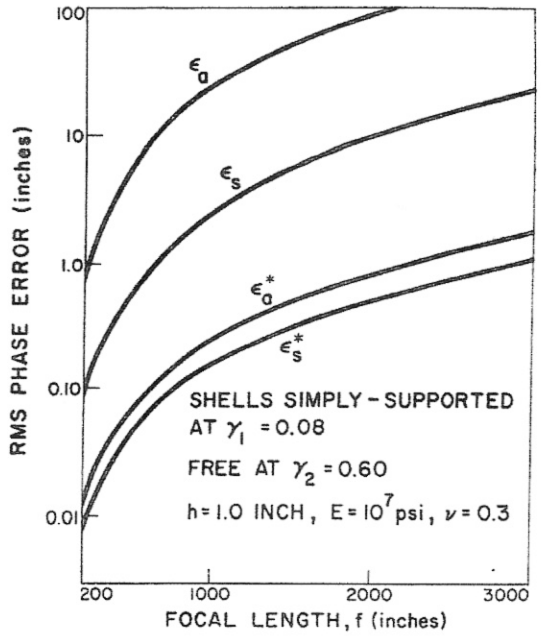


Fig. 21. Effect of focal length

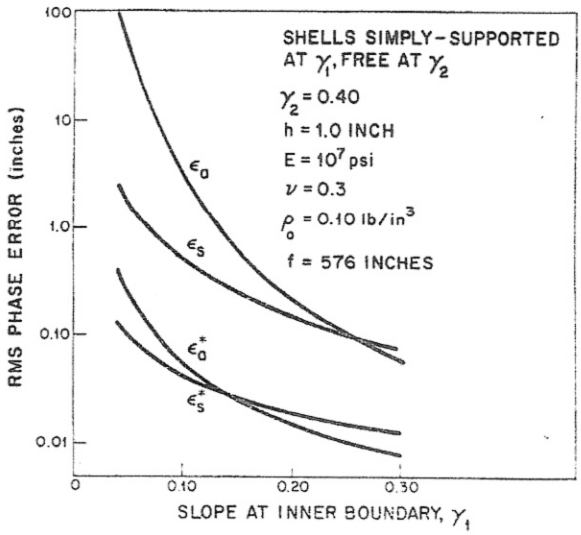


Fig. 22. Effect of location of inner boundary

One set is free at an outer boundary with a slope of 0.4 while the other is free at an outer boundary with a slope of 0.6. Figures 22 and 23 summarize the results. Each figure consists of four curves, two of which refer to the RMS of the total deflection and two to the effective deflection. Again we

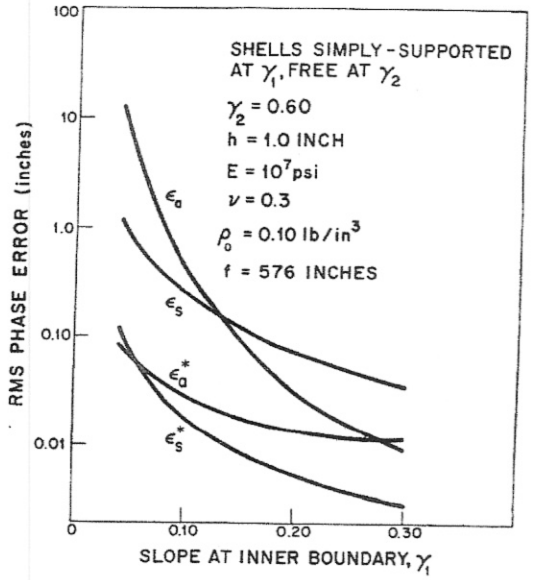


Fig. 23. Effect of location of inner boundary

observe that despite an order of magnitude difference between face-up and face-side results for phase error as based on the total deflection, the phase errors when rigid-body displacements are subtracted are comparable. Also, the very large deflections in the face-side attitude are due mainly to rigid body rotations.

### Type of support

The supported boundary for the shells studied in the previous sections have all been simply-supported. This means for the symmetric case

$$u = w = M_r = 0 \tag{60}$$

and for the antisymmetric case

$$u = v = w = M_r = 0. \tag{61}$$

In this section the effect of three other boundary support conditions will be considered. These will be referred to as clamped, roller, and membrane. In terms of shell theory these have the following mathematical representation. For the symmetric attitude

Clamped: $$u = w = \omega_r = 0 \tag{62}$$

Roller: $$M_r = u_r \sin\phi + w\cos\phi = N_r\cos\phi - Q_r\sin\phi = 0 \tag{63}$$

Membrane: $$u = M_r = Q_r = 0. \tag{64}$$

For the antisymmetric attitude

Clamped: $$u = v = w = \omega_r = 0 \tag{65}$$

Roller: $$M_r = u_r\sin\phi + w\cos\phi = N_r\cos\phi$$
$$-\left(Q_r + \frac{1}{2f\gamma}\frac{\partial M_{r\theta}}{\partial\theta}\right)\sin\phi = N_{r\theta} + \frac{M_{r\theta}}{2f\sqrt{1+\gamma^2}} = 0 \tag{66}$$

Membrane: $$u = v = Q_r + \frac{1}{r}\frac{\partial M_{r\theta}}{\partial\theta} = M_r = 0. \tag{67}$$

The membrane type of support has been previously discussed and is schematically shown in Fig. 8. The clamped and roller supports are schematically shown in Fig. 24.

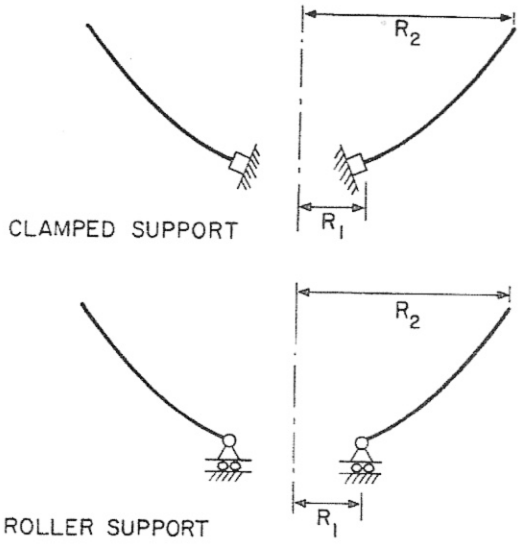


Fig. 24

The results of a series of calculations are shown plotted in Figs. 25 and 26 for the symmetric ($\psi = 0°$) and antisymmetric ($\psi = 90°$) cases, respectively. Only the $\varepsilon_s^*$ and $\varepsilon_a^*$ values which are based on the effective displacements have been plotted. It is observed that the membrane type of support provides the smallest $\varepsilon$ and $\varepsilon^*$. Somewhat surprisingly (at first glance) the roller support is the worst. However this can be attributed to the large transverse shears developed at the roller support.

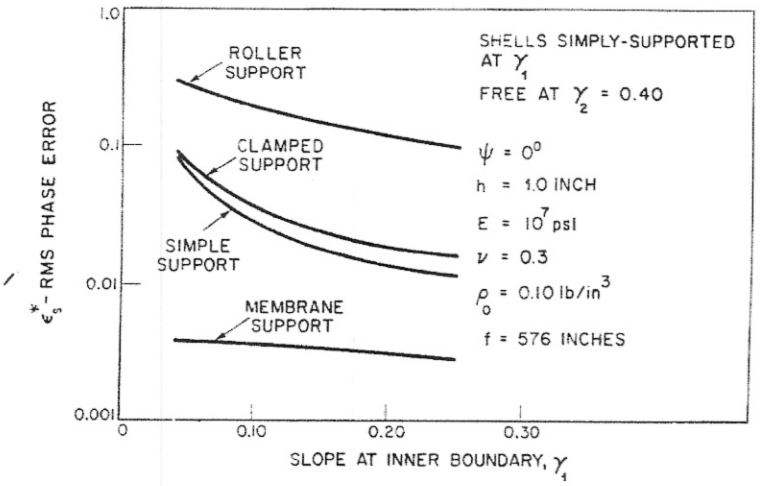


Fig. 25. Effect of support conditions

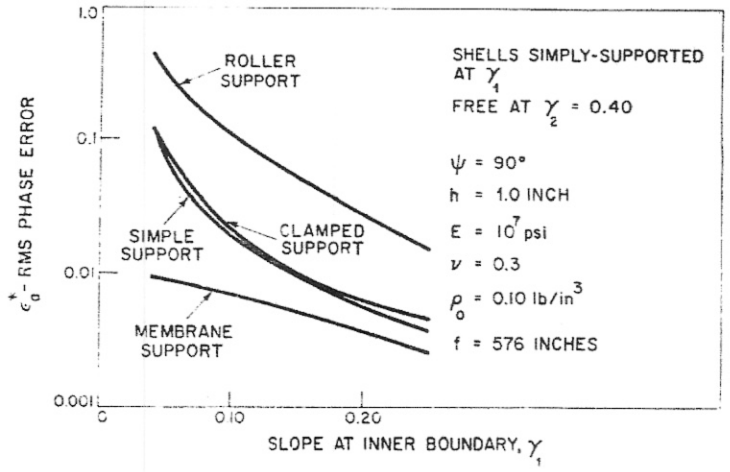


Fig. 26. Effect of support conditions

It is also interesting that the clamped support and the simple support yield approximately the same RMS phase errors with the clamped support showing slightly larger errors. This can be attributed to the larger bending moments induced in the edge zone by the clamped support.

### Interior support

The interior support configuration is schematically shown in Fig. 27. At the support radius, $R_s$, the shell is continuous, i.e. the displacements $u, v, w$ and the rotation $\omega_r$ are continuous across $R_s$. Two shells with

their support radii at $\gamma_s = 0.14$ ($R_s = 161.28$ in.) and $\gamma_s = 0.20$ ($R_s = 230.4$ in.), respectively, and free at $\gamma_2 = 0.60$ ($R_2 = 691.20$ in.) have been analyzed. Both the total and effective deflection curves are shown in

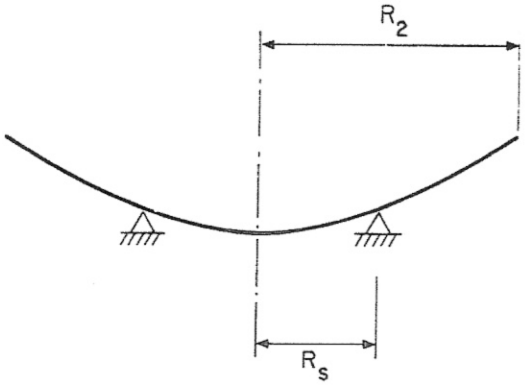


Fig. 27. Interior support configuration

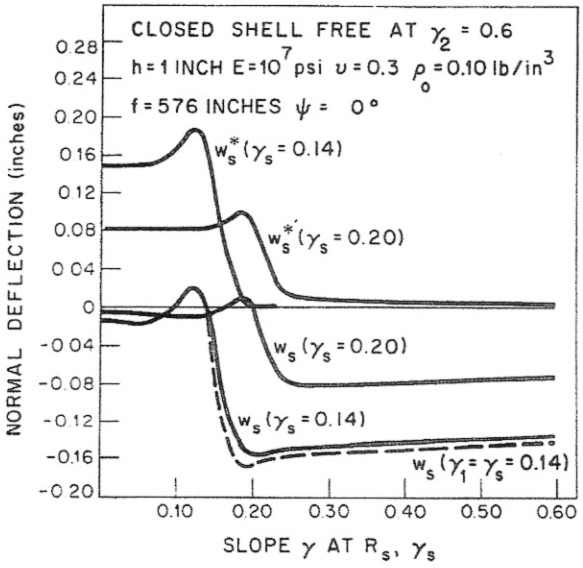


Fig. 28

Figs. 28 and 29 for the symmetric and antisymmetric cases, respectively. The results are consistent with those of the other sections; the deflections become smaller as the radius of support becomes larger. Of greater importance is the small effect provided by the continuity of the shell. The dashed curves in Figs. 28 and 29 are the deflections for a shell simply-supported

at a slope of 0.14 ($R_1 = 161.28$ in.) and free at a slope of 0.60 ($R_2 = 691.20$ in.). Their close proximity to the curves for a closed shell with an interior support at a radius of $R_s = 161.28$ in. indicates the very small changes in deflections provided by an interior support. The explanation lies in the

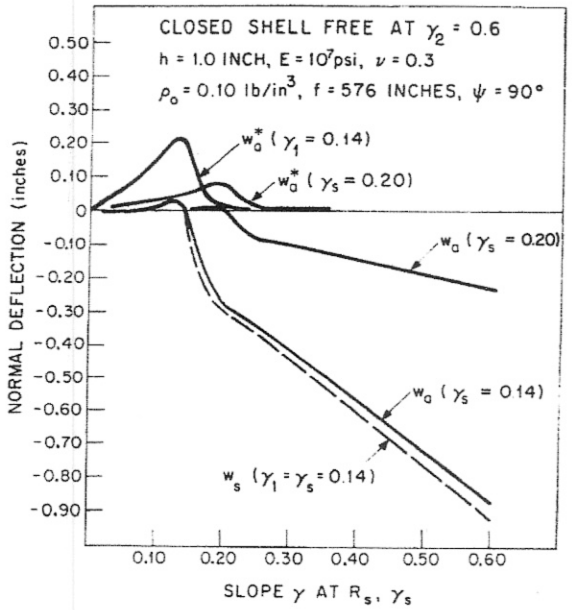


Fig. 29. Effect of interior support

small percentage of the total span occupied by the edge zone bending. Not shown in this paper are the rather substantial bending moments engendered by making the shell continuous over a support.

### 4. On the Construction of the Reflector

In the foregoing discussion, we have tacitly assumed that the shell is supported everywhere during construction. Usually the reflector is in the face-up position during this period. After the supports are removed (effectively, gravity is turned on), the shell experiences a deformation whose normal component we have called $w_s$. As the pointing angle $\psi$ changes, the normal deflection is given by (see Eqs. 12 and 49)

$$w(\gamma, \theta, \psi) = w_s(\gamma)\cos\psi + w_a(\gamma)\sin\theta\sin\psi. \tag{68}$$

Correspondingly, the RMS phase error (with respect to the moved paraboloid) is given by

$$\varepsilon^*(\psi) = \{\cos^2\psi\varepsilon_s^{*2} + \sin^2\psi\varepsilon_a^{*2}\}^{\frac{1}{2}}. \tag{69}$$

The latter error is a function only of $\psi$ since $\varepsilon_s^*$ and $\varepsilon_a^*$ are just two numbers for a prescribed antenna geometry and material.

The antenna can also be built in such a way that after the construction supports are removed the reflector becomes a perfect paraboloid in the face-up position. For such a construction procedure, the normal deflection experienced by the dish at some arbitrary angle $\psi$ is

$$\tilde{w}(\gamma, \theta, \psi) = w_s(\gamma)(\cos\psi - 1) + w_a(\gamma)\sin\psi\sin\theta \tag{70}$$

Correspondingly we have

$$\tilde{\varepsilon}^*(\psi) = \{(\cos\psi - 1)^2\varepsilon_s^{*2} + \sin^2\psi\,\varepsilon_a^{*2}\}^{\frac{1}{2}}. \tag{71}$$

A comparison of the two methods of construction has been made by plotting Eqs. (69) and (71) normalized as follows:

$$\frac{\varepsilon^*(\psi)}{\varepsilon_a^*} = \{\cos^2\psi x^2 + \sin^2\psi\}^{\frac{1}{2}} \tag{72}$$

$$\frac{\tilde{\varepsilon}^*(\psi)}{\varepsilon_a^*} = \{(\cos\psi - 1)^2 x^2 + \sin^2\psi\}^{\frac{1}{2}} \tag{73}$$

where

$$x = \frac{\varepsilon_s^*}{\varepsilon_a^*}. \tag{74}$$

These two equations are shown plotted in Fig. 30 for several ratios of $x$. This figure shows that $\tilde{\varepsilon}^*(\psi)/\varepsilon_a^*$ is smaller than $\varepsilon^*(\psi)/\varepsilon_a^*$ for $\psi = 0°$. The difference becomes less and less significant as $\psi$ increases and is in fact equal

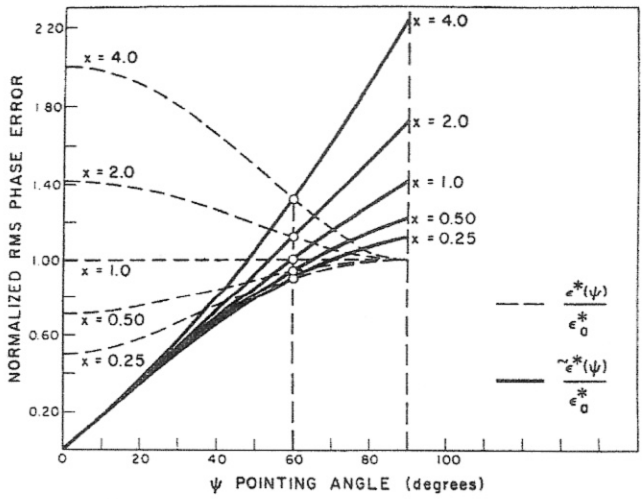


Fig. 30. Variation of error with pointing angle

to zero at $\psi = 60°$. For larger values of $\psi$, $\tilde{\varepsilon}^*(\psi)/\varepsilon_a^*$ is greater than $\varepsilon^*(\psi)/\varepsilon_a^*$. The implications of these plots are twofold. Firstly, depending on the most frequently used pointing angles we may or may not want to set the surface

at its true shape in the face-up position. Secondly, a better performance may be possible by constructing the antenna so that it attains the perfect paraboloidal shape at some optimal angle $\psi_0$. Clearly, if only the horizon is to be viewed by the antenna then the shell should be so built that the desired paraboloidal shape is attained at $\psi = 90°$. For this construction, the normal deformation is given by

$$\hat{w}(\gamma, \theta, \psi) = w_s(\gamma)\cos\psi + w_a(\gamma)\sin\theta(\sin\psi - 1) \tag{75}$$

while the corresponding RMS phase error (with respect to the moved paraboloid) is

$$\hat{\varepsilon}^*(\psi) = \{\cos^2\psi\, \varepsilon_s^{*2} + (\sin\psi - 1)^2 \varepsilon_a^{*2}\}^{\frac{1}{2}}. \tag{76}$$

A comparison of this latter method of construction with the first method has been made by comparing Eqs. (76) and (69), with Eq. (76) normalized as follows

$$\frac{\hat{\varepsilon}^*(\psi)}{\varepsilon_a^*} = \{\cos^2\psi x^2 + (\sin\psi - 1)^2\}^{\frac{1}{2}}. \tag{77}$$

Equation (77) and Eq. (72) are shown for several values of $x$ in Fig. 31. It can be seen that $\hat{\varepsilon}^*$ is always smaller than $\varepsilon^*$ for $\psi > 30°$ while the opposite is true for $\psi \leqslant 30°$.

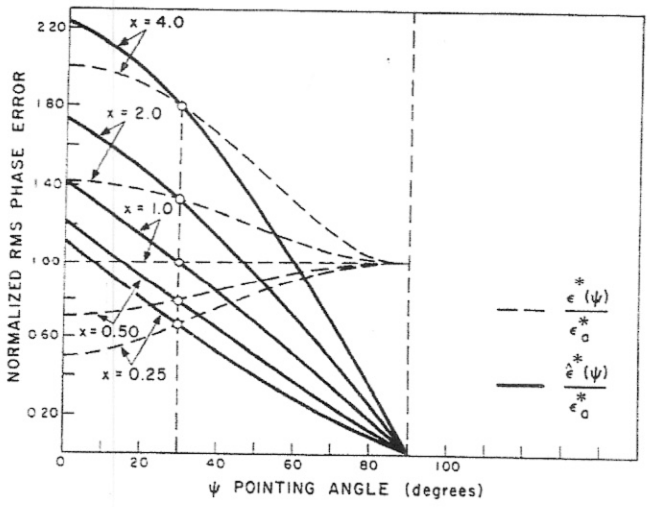


Fig. 31. Variation of error with pointing angle

The quantities $\tilde{\varepsilon}^*$ and $\hat{\varepsilon}^*$ represent the two extremes between which the optimal angle $\psi_0$ must lie. Together with an intermediate reference $\varepsilon^*$ they serve as guides for optimization.

## 5. Concluding Remarks

We have presented here some results which, we hope, will contribute to a better understanding of the structural behavior of the reflecting surface. The implementation of these results in a practical structure presents engineering problems which remain to be investigated. If the antenna shell can be supported at its edges in the manner specified by the mathematically stated boundary conditions, e.g., zero deflection and zero bending moment, then the shell will behave as depicted. However, the provision of a simple-support at a radius of several hundred inches from the axis of revolution creates formidable design and construction problems.

No study of the structural aspect of an antenna is complete without a study of the back-up structure required to support the reflecting surface. There are many tools available (e.g., Ref. 7) to analyze the spaceframe type of back-up structure. Only by analyzing the shell, the back-up structure and their interaction can the true system implications of each component on the optimum design of large antennae be properly assessed.

There are other system engineering problems which need to be included before a true appraisal of an optimum design can be made. The illumination of the antenna surface, the support of the focal point, and the manner by which the radio-astronomer electrically determines the performance of the antenna are important considerations. A major engineering feat which requires a solution is the measurement of the shape of the reflecting surface. Finally, costs of competing ideas are always significant. These and other factors which are part and parcel of the complete system are beyond the scope of this paper.

## References

[1] WEISS, H. G., The Haystack microwave research facility, *IEEE Spectrum* **2**, 50–69 (February 1965)

[2] MAR, J. W. and WAN, F. Y. M., Distortions and Stresses of Paraboloidal Surface Structures, Part II, Lincoln Laboratory Report 71G-1 (January 1963)

[3] MAR, J. W. and WAN, F. Y. M., Distortions and Stresses of Paraboloidal Surface Structures, Part III, Lincoln Laboratory Report 71G-1 (August 1963)

[4] MAR, J. W. and WAN, F. Y. M., Distortions and Stresses of Paraboloidal Surface Structures, Part IV, Lincoln Laboratory Report 71G-1 (April 1964)

[5] MAR, J. W. and WAN, F. Y. M., Comparative Analyses of Thin Paraboloidal Shells of Revolution Under Gravity Load, Proceedings of the World Conference on Shell Structures, pp. 487–499, National Academy of Science Press (1964)

[6] DION, A. R., Investigation of Effects of Surface Deviations on Haystack Antenna Radiation Patterns, Lincoln Laboratory Report TR-324 (July 1963)

[7] M. I. T. Lincoln Laboratory, STAIR Instruction Manual, Lincoln Manual No. 48 (March 1962)

[8] RUZE, J., The Effect of Aperture Errors on the Antenna Radiation Pattern, Supplemento AL V. IX, Ser. IX, *Del nuovo cimento*, No. 3 (1952)